

Ordered phases in the Holstein-Hubbard model: Interplay of strong Coulomb interaction and electron-phonon coupling

Yuta Murakami,¹ Philipp Werner,² Naoto Tsuji,¹ and Hideo Aoki¹

¹*Department of Physics, University of Tokyo, Hongo, Tokyo 113-0033, Japan*

²*Department of Physics, University of Fribourg, 1700 Fribourg, Switzerland*

(Dated: November 5, 2018)

We study the Holstein-Hubbard model at half filling to explore ordered phases including superconductivity (SC), antiferromagnetism (AF), and charge order (CO) in situations where the electron-electron and electron-phonon interactions are strong (\sim electronic bandwidth). The model is solved in the dynamical mean-field approximation using a continuous-time quantum Monte Carlo impurity solver. We determine the superconducting transition temperature (T_c) and the SC order parameter and show that the phonon-induced retardation or the strong Coulomb interaction leads to a significant reduction and shift of the T_c dome if one interprets the system as having an effective static interaction U_{eff} given by the Hubbard U reduced by the phonon-mediated attraction in the static limit. This behavior is analyzed by comparison to an effective static model in the polaron representation with a reduced bandwidth. We also determine the finite-temperature phase diagram including AF and CO. In the moderate-coupling regime, there is a hysteretic region of AF and CO around $U_{\text{eff}} = 0$, while the two phases are separated by a paramagnetic metal in the weak-coupling regime and a paramagnetic insulator in the strong coupling regime.

PACS numbers: 71.38.-k, 71.10.Fd, 71.10.-w, 74.20.-z

I. INTRODUCTION

While the physics of correlated electron systems is an interesting and formidable problem in its own right, several classes of interesting materials exhibit an interplay of strong electron-electron Coulomb repulsion and strong electron-phonon coupling. For example, the electron-phonon coupling in high- T_c cuprates is strong, as evidenced by the kinks observed in the angle-resolved photoemission spectrum.¹ In alkali-doped fullerenes an s -wave superconducting phase borders an antiferromagnetic phase in the temperature-pressure phase diagram²⁻⁴ and the transition temperature of the superconducting state has recently been found to be dome-shaped. These features indicate that in these classes of materials, both the electron-electron Coulomb repulsion and the electron-phonon interaction are strong. Likewise, in aromatic superconductors such as picene (a recent addition to carbon-based materials), the electron-electron and electron-phonon interactions are reported to be strong,⁵⁻⁷ although the mechanism of superconductivity in the aromatic compounds is still totally unclear. Correlated electron systems often provide an interesting arena in which various phases compete with each other. In the presence of strong electron-electron and electron-phonon interactions, the problem should become even richer.

The Holstein-Hubbard (HH) model is a simple model which allows to describe and explore the interplay of electron-electron and electron-phonon interactions. The model incorporates a coupling between electrons and dispersionless (i.e., Einstein) phonons with energy ω_0 , in addition to the on-site Hubbard interaction U . There is a body of works which investigates the competition between the two interactions in this model. The study of the one-dimensional case based on the density matrix renormalization group (DMRG) technique or quantum Monte Carlo analysis has revealed some general

features.⁸⁻¹⁰ However, since ordered phases with continuous symmetry breaking do not occur in $D = 1$, it is difficult to elucidate the generic behavior of ordered states from these calculations, although we can indeed discuss quasi-ordered states in terms of the Tomonaga-Luttinger picture. In the opposite limit of infinite spatial dimensions, $D = \infty$, where the dynamical mean-field theory (DMFT) becomes exact,¹¹⁻¹³ ordered states with full symmetry breaking exist even at nonzero temperature. The effect of the competition between the two kinds of interactions on symmetric phases have been studied in Refs. 14–17, and the corresponding phase diagram has been determined.

As for the ordered states, their properties have been investigated in several works,¹⁸⁻²² but many issues remain unresolved. The ground state phase diagram around $U = \lambda$, where λ is the static effective electron-electron interaction mediated by the phonons, has been determined in Refs. 19, 20, and deviations from the conventional theory of superconductivity have been discussed.^{21, 22} An important issue is the following: the electron-phonon coupled system is often regarded as having an effective interaction $U_{\text{eff}} \equiv U - \lambda$, but this is only strictly valid in the antiadiabatic limit for the phonon energy, $\omega_0 \rightarrow \infty$, where the interaction in the HH model becomes non-retarded, and the real question is to what extent this approximation remains valid when we vary U and/or ω_0 . In other words, for a finite ω_0 the phonon-mediated interaction is certainly retarded, and for small enough phonon frequency, the static model with U_{eff} can be expected to fail. Thus the nature of the superconducting state in the regime where U , λ , and ω_0 are all comparable to the bandwidth W poses an challenging problem, which is not only conceptually interesting, but may have relevance to real materials with strong electron-electron and electron-phonon interactions. The problem, however, has not been properly understood, since superconducting states in such a regime cannot be treated within conventional theories such as the Migdal theorem^{23, 24}

or the MacMillan equation.²⁵ Another open issue is the finite-temperature phase diagram for ordered phases in the vicinity of $U = \lambda$.

With these questions in mind, we study in this paper ordered states in the half-filled Holstein-Hubbard model to clarify the effect of the coexistence of electron-electron and electron-phonon interactions on the s -wave superconducting state (SC), the antiferromagnetic (AF) state and the charge ordered state (CO). In our study we employ DMFT, with a continuous-time quantum Monte Carlo (CT-QMC) impurity solver, which is exact up to statistical errors, and can in principle access any parameter regime down to temperatures of about one percent of the electronic bandwidth. Furthermore, DMFT + CT-QMC can treat these three ordered states without bias, which enables us to systematically investigate their competition in the regime where U , λ , and ω_0 are comparable to the bandwidth. Note that even though there have been several works discussing ordered states in HH model,^{18–20,22} the present work is, to the best of our knowledge, the first attempt to directly treat these ordered phases at non-zero temperatures with DMFT+CT-QMC. For SC, we focus on the transition temperature and the superconducting order parameter. We show that the phonon-induced retardation (when the phonon energy is well below the antiadiabatic limit) or the Coulomb repulsion have the effect of significantly decreasing and shifting the T_c dome against U_{eff} , and a similar shift occurs for the superconducting order parameter as well. In order to understand and interpret the observed behavior we use an effective static model in a polaron representation with reduced bandwidth derived from a Lang-Firsov transformation, which has been introduced to investigate electron-phonon coupled systems in the strong-coupling or antiadiabatic regime.^{26–28} We test the quantitative and qualitative reliability of the effective model by examining to what extent the model reproduces the transition temperature, superconducting order parameter and Green's function. As for AF and CO phases, we determine the phase diagram at nonzero temperature, and show how these phases compete with each other at moderate to strong couplings.

The paper is organized as follows. In Sec. II, we introduce the Holstein-Hubbard model and explain how DMFT can deal with ordered phases of this model. We also derive the effective static model. In Sec. III, we discuss how the properties of the superconducting state depend on the parameters U , λ , and ω_0 when these parameters are comparable to the bandwidth. We also show phase diagrams at nonzero temperatures around $U = \lambda$, and reveal how AF and CO compete with each other. Sec. IV gives a brief summary.

II. FORMALISM

A. Model

The Holstein-Hubbard (HH) model represents an electron system that is coupled to local (Einstein) phonons.

The Hamiltonian is

$$H = -t \sum_{\langle i,j \rangle, \sigma} [c_{j\sigma}^\dagger c_{i\sigma} + H.c.] + \sum_i [U n_{i\uparrow} n_{i\downarrow} - \mu(n_{i\uparrow} + n_{i\downarrow})] + g \sum_i (b_i^\dagger + b_i)(n_{i\uparrow} + n_{i\downarrow} - 1) + \omega_0 \sum_i b_i^\dagger b_i, \quad (1)$$

where i, j denote sites, σ the spin, and the first sum is over nearest neighbors. $c_{i,\sigma}^\dagger$ denotes a creation operator of an electron, b_i^\dagger a creation operator of a phonon, t the hopping parameter, U the on-site electron-electron interaction, μ the chemical potential, g the coupling constant between electrons and phonons and ω_0 the phonon frequency. In this model, the phonon is envisaged as an optical mode with an approximately constant energy dispersion (Einstein model). Since the phonons are assumed to be noninteracting, one can integrate out the phonon part to derive the effective electron-electron interaction,

$$U_{\text{eff}}(\omega) = U - \frac{2g^2\omega_0}{\omega_0^2 - \omega^2}, \quad (2)$$

in a path integral framework. The effective interaction in the low-energy regime is thus

$$U_{\text{eff}} \equiv U_{\text{eff}}(\omega = 0) \equiv U - \lambda, \quad \lambda = 2g^2/\omega_0. \quad (3)$$

If we take the anti-adiabatic limit of $\omega_0 \rightarrow \infty$ with λ and U fixed, the HH model reduces to the Hubbard model with the interaction U_{eff} . This low-energy effective interaction has been used as a measure of the characteristic effective net interaction in previous works.^{8,19,20} In the present work we examine the validity of a static description in the parameter regime of interest, namely strong electron-electron and electron-phonon coupling, with phonon frequencies comparable to the bandwidth. We shall see that a proper static description involves the screened interaction, along with a reduced bandwidth.

In order to deal with superconducting (SC) states, we employ the Nambu formalism and define the local Green's function as

$$\hat{G}_{\text{loc},i}(\tau) \equiv -\langle T \Psi_i(\tau) \Psi_i^\dagger(0) \rangle = \begin{bmatrix} G_{11,i}(\tau) & G_{12,i}(\tau) \\ G_{21,i}(\tau) & G_{22,i}(\tau) \end{bmatrix}, \quad (4)$$

where $\Psi_i^\dagger \equiv (c_{i\uparrow}^\dagger, c_{i\downarrow})$ are Nambu spinors. We use

$$\Phi = \langle c_{i\downarrow} c_{i\uparrow} \rangle_H = G_{12}(\tau = 0_+), \quad (5)$$

as the order parameter for the SC phase (assuming homogeneity), where $\langle \rangle_H$ denotes the equilibrium expectation value computed with the Hamiltonian H .

B. Dynamical mean-field theory

The dynamical mean-field theory (DMFT), which is exact in infinite spatial dimensions,^{11–13} maps a lattice problem onto an effective impurity problem. When we take into account the superconducting state of the Holstein-Hubbard model, the Hamiltonian of the impu-

rity problem is $H_{\text{imp}} = H_{\text{loc}} + H_{\text{bath}} + H_{\text{mix}}$, with the three terms

$$H_{\text{loc}} = U n_{\uparrow} n_{\downarrow} - \mu (n_{\uparrow} + n_{\downarrow}) + g(b^{\dagger} + b)(n_{\uparrow} + n_{\downarrow} - 1) + \omega_0 b^{\dagger} b, \quad (6)$$

$$H_{\text{bath}} = \sum_{\sigma, p} \epsilon_p c_{p, \sigma}^{\dagger} c_{p, \sigma} + \sum_p (\Delta_p c_{p \uparrow}^{\dagger} c_{-p \downarrow}^{\dagger} + \text{H.c.}), \quad (7)$$

$$H_{\text{mix}} = \sum_{\sigma, p} (V_p^{\sigma} d_{\sigma}^{\dagger} c_{p, \sigma} + \text{H.c.}). \quad (8)$$

Here d is the annihilation operator of the electron on the impurity, n_{σ} the density of electrons with spin σ on the impurity, b the annihilation operator of a local phonon coupled to the impurity, and c the annihilation operator of an electron in the bath, with the bath states labeled by the quantum number p . In a SC state the parameters Δ_p can be nonzero. Thus the Hamiltonian describes an impurity that is coupled to local phonons in a superconducting bath. The bath (H_{bath}) and mixing (H_{mix}) terms are determined self-consistently in such a way that the impurity Green's function reproduces the local lattice Green's function of the HH model. The only information on the lattice structure that enters a DMFT calculation is the density of states. Here we adopt the Bethe lattice, whose density of states is $\rho(\epsilon) = \frac{1}{\pi t} \sqrt{1 - (\epsilon/(2t))^2}$. We use the quarter of the bandwidth, t , as the unit of energy.

Since we want to describe phases such as antiferromagnetic (AF) and charge-ordered (CO) ones with a broken Z_2 symmetry between sublattices, we introduce sub-lattice indices $\theta = A, B$ ($\theta = B, A$) (here for the Bethe lattice, which is bipartite) and express the self-consistency equation in the form

$$\begin{aligned} [\hat{\Lambda}_{\theta}]_{i,j}(\tau) &= -\langle T A_i(\tau) A_j^{\dagger}(0) \rangle_{H_{\text{bath}}} \\ &= [t^2 \sigma_3 \hat{G}_{\text{loc} \theta}(\tau) \sigma_3]_{i,j}, \end{aligned} \quad (9)$$

where $\hat{\Lambda}$ is the hybridization function of the impurity model. Here, $A_i = \sum_p V_p^i a_{p,i}$, $V_p^1 = V_p^{\uparrow}$, $V_p^2 = -V_p^{\downarrow}$, $(a_{p,1}^{\dagger}, a_{p,2}^{\dagger}) \equiv (c_{p,\uparrow}^{\dagger}, c_{-p,\downarrow}^{\dagger})$ (all quantities for sublattice θ), and $\sigma_3 = \text{diag}(1, -1)$ is a Pauli matrix. If we assume a homogenous system, as in the investigation of SC, then $\hat{\Lambda}_{\theta}(\tau) = \hat{\Lambda}(\tau)$ is independent of the sublattice.

The impurity problem, Eqs. (6)-(8) is solved with the continuous-time Quantum Monte Carlo impurity solver (hybridization expansion, i.e. we regard the mixing term (8) as a perturbation term and perform a Monte Carlo sampling of the corresponding diagrammatic expansion),^{29,30} based on the method introduced in Ref. 14. In this approach, a Lang-Firsov decoupling³¹ of the electrons and phonons and an analytical summation of all phonon contributions for each term in the expansion of the hybridization term enables an exact treatment of the quantum phonons. In the present case, we extend this technique to impurity problems that couple to a superconducting bath.³⁶

C. Effective static model

Before presenting the DMFT results, let us first introduce an effective static model for the low-energy description of the HH model,^{26,28} which is useful for discussing the properties of the SC phase. The first step in the derivation is to perform a Lang-Firsov (LF) canonical transformation for the HH model, $H_{\text{LF}} = e^S H e^{-S}$ with $S = \frac{g}{\omega_0} \sum_{i, \sigma} n_{i, \sigma} (b_i^{\dagger} - b_i)$. The explicit expression of H_{LF} is

$$\begin{aligned} H_{\text{LF}} &= -t \sum_{\langle i, j \rangle, \sigma} [e^{\frac{g}{\omega_0} (b_i^{\dagger} - b_i)} e^{-\frac{g}{\omega_0} (b_j^{\dagger} - b_j)} c_{i, \sigma}^{\dagger} c_{j, \sigma} + \text{H.c.}] \\ &+ U_{\text{eff}} \sum_i n_{i, \uparrow} n_{i, \downarrow} + \mu_{\text{eff}} \sum_i n_i + \omega_0 \sum_i b_i^{\dagger} b_i, \end{aligned} \quad (10)$$

where $\mu_{\text{eff}} = \mu - \frac{g^2}{\omega_0}$. Here, c^{\dagger} , after the LF transformation, has a meaning of creating a polaron, as is evident from the phonon factors. An effective low-energy model for the original fermions is obtained by assuming that the phonons are not much excited. In other words, the effective Hamiltonian for the fermion part is obtained as the projection onto the subspace of zero phonons, $H_{\text{eff}} = \langle 0 | H_{\text{LF}} | 0 \rangle$, where $|0\rangle$ is the vacuum of phonons. This description becomes exact in the limit where ω_0 is large and the temperature is much lower than ω_0 . The Hamiltonian resulting from this projection is²⁶

$$\begin{aligned} H_{\text{eff}} &= -Z_B t \sum_{\langle i, j \rangle, \sigma} [c_{i, \sigma}^{\dagger} c_{j, \sigma} + \text{H.c.}] \\ &+ U_{\text{eff}} \sum_i n_{i, \uparrow} n_{i, \downarrow} + \mu_{\text{eff}} \sum_i n_i, \\ Z_B &= \exp(-g^2/\omega_0^2). \end{aligned} \quad (11)$$

This is nothing but the usual Hubbard model with a static interaction U_{eff} and a hopping parameter renormalized by Z_B . For this model we can readily derive physical quantities such as the transition temperature, the order parameter for the SC phase or the Green's functions from simulations of the Hubbard model as follows.

Let us define $\Phi(T, U, U_{\text{eff}}, Z_B) = \langle c_{\downarrow} c_{\uparrow} \rangle_H$ as the order parameter for the SC state. Within the effective model, the order parameter is expressed as

$$\begin{aligned} \Phi(T, U, U_{\text{eff}}, Z_B) &= \langle e^{-2\frac{g}{\omega_0} (b^{\dagger} - b)} c_{\downarrow} c_{\uparrow} \rangle_{H_{\text{LF}}} \approx \\ &\langle 0 | e^{-2\frac{g}{\omega_0} (b^{\dagger} - b)} | 0 \rangle \langle c_{\downarrow} c_{\uparrow} \rangle_{H_{\text{eff}}} = Z_B^2 \Phi_0(T/Z_B, U_{\text{eff}}/Z_B) \\ &\equiv \Phi_{\text{eff}}[Z_B, U_{\text{eff}}], \end{aligned} \quad (12)$$

where we have defined $\Phi_0(T, U)$ as the order parameter for the Hubbard model with hopping t and interaction U at temperature T . It follows that the transition temperature for the Holstein-Hubbard model ($T_c[U, U_{\text{eff}}, Z_B]$) is related to that for the attractive Hubbard model ($T_c^0[U]$)

by

$$\begin{aligned} T_c[U, U_{\text{eff}}, Z_B] &\approx Z_B \times T_c^0[U_{\text{eff}}/Z_B] \\ &\equiv T_{c,\text{eff}}[Z_B, U_{\text{eff}}]. \end{aligned} \quad (13)$$

In order to evaluate Green's functions, we again use the LF transformation,

$$\begin{aligned} G_\sigma(\tau) &= -\langle T_\tau c_\sigma(\tau) c_\sigma^\dagger(0) \rangle_H \\ &= -\langle T_\tau e^{-\frac{g}{\omega_0}(b^\dagger(\tau)-b(\tau))} e^{\frac{g}{\omega_0}(b^\dagger(0)-b(0))} c_\sigma(\tau) c_\sigma^\dagger(0) \rangle_{H_{LF}}. \end{aligned} \quad (14)$$

Then we employ an approximation, which is to separate out the phonon factors from the expectation value with respect to H_{LF} (in the situation where ω_0 is large the phonon dynamics may be decoupled from the polaron dynamics). The fermionic part is evaluated by the static approximation. This gives

$$\begin{aligned} G_\sigma(\tau) &\approx -\langle T_\tau c_\sigma(\tau) c_\sigma^\dagger(0) \rangle_{H_{\text{eff}}} \\ &\times \langle T_\tau e^{-\frac{g}{\omega_0}(b^\dagger(\tau)-b(\tau))} e^{\frac{g}{\omega_0}(b^\dagger(0)-b(0))} \rangle_{H_{\text{ph}}}, \end{aligned} \quad (15)$$

where $H_{\text{ph}} = \omega_0 \sum_i b_i^\dagger b_i$. In other words, we treat the whole system as if its Hamiltonian is $H_{\text{eff}} + H_{\text{ph}}$.²⁷

As for the anomalous part,

$$\begin{aligned} G_{12}(\tau) &\approx -\langle T_\tau c_\uparrow(\tau) c_\downarrow(0) \rangle_{H_{\text{eff}}} \\ &\times \langle T_\tau e^{-\frac{g}{\omega_0}(b^\dagger(\tau)-b(\tau))} e^{-\frac{g}{\omega_0}(b^\dagger(0)-b(0))} \rangle_{H_{\text{ph}}}. \end{aligned} \quad (16)$$

The phonon factor can be calculated analytically as

$$\begin{aligned} &\langle T_\tau e^{-s\frac{g}{\omega_0}(b^\dagger(\tau)-b(\tau))} e^{-s'\frac{g}{\omega_0}(b^\dagger(0)-b(0))} \rangle_{H_{\text{ph}}} \\ &= \exp\left\{-\frac{g^2/\omega_0^2}{e^{\beta\omega_0}-1} [(e^{\omega_0\beta}+1) + ss'(e^{\omega_0(\beta-\tau)} + e^{\omega_0\tau})]\right\}, \end{aligned} \quad (17)$$

where $s, s' = \pm 1$ and $0 \leq \tau \leq \beta$.

III. RESULTS

A. Superconductivity

Here, we investigate the SC phase at half-filling, in order to understand the effect of the retardation and the Coulomb repulsion on the SC state. To focus on SC, we enforce the symmetries $G_{11}(\tau) = G_{11}(\beta - \tau) = G_{22}(\tau) = G_{22}(\beta - \tau)$, which hold in the SC and normal states at half filling, but not in the AF and CO phases. Strictly speaking, if we allow both CO and SC orders in the self-consistency loop, CO dominates over SC. Still, it should be meaningful to study the SC state at half-filling, since, if the system has a frustration (e.g. induced by a second-neighbor hopping on a bipartite lattice), CO and AF may be suppressed. The results of this subsection can be thought of as describing the properties of such frustrated systems.

We first show that the Coulomb interaction induces a

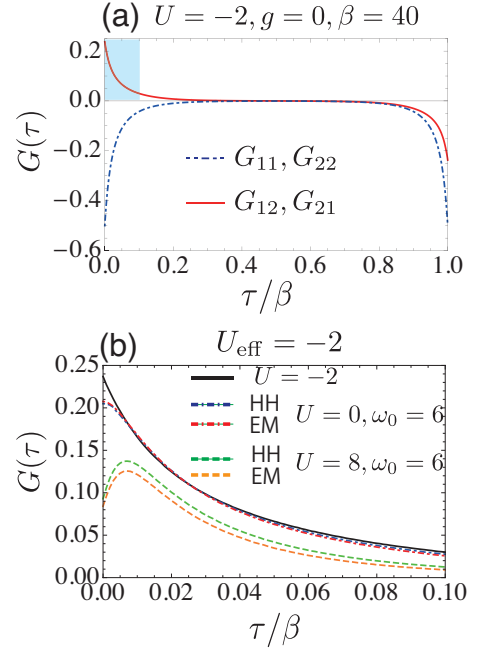


FIG. 1: (a) Typical behavior of Green's functions on the imaginary time axis, here for $U = -2$, $g = 0$, and $\beta = 40$. (b) A close-up (blue region in (a)) of the anomalous Green's function for various cases for fixed $U_{\text{eff}} = -2$, where g and U are changed to keep U_{eff} const with $\omega_0 = 6$ and $\beta = 40$. 'HH' means the Green's function is computed from the HH model, while 'EM' means that it is obtained with the effective model.

characteristic structure in the anomalous Green's function. Figure 1(a) plots normal and anomalous Green's functions on the imaginary-time axis. While the diagonal Green's functions are negative and symmetric (at half-filling), the off-diagonal Green's functions are anti-symmetric around $\tau/\beta = 0.5$. In Fig. 1(b) we show the short-time behavior of the anomalous Green's functions for different sets of parameter values: without retardation (Hubbard model with $U = -2$), with only a retarded attractive interaction ($U = 0$ and $\omega_0 > 0$) and with both retardation and Coulomb repulsion. In all three cases, $U_{\text{eff}} = -2$, $\omega_0 = 6$ and $T = 0.025$. Without the retardation, the anomalous Green's function has its maximum at $\tau = 0$. In the presence of a retarded attractive interaction, but without U , the position of the maximum remains at $\tau = 0$, but the initial peak is rounded off. If we then switch on a $U > 0$, the peak shifts to $\tau > 0$, which indicates that when electrons form pairs, they tend to avoid the instantaneous repulsive interaction U while exploiting the retarded attractive interaction.

One can explain the origin of this behavior with the effective model, Eq.(16). The corresponding results are also shown in Fig.1(b). It turns out that the shift of the peak with U in the anomalous Green's function is well reproduced by the effective model. This structure comes from the phonon part, Eq. (17), which increases with τ near $\tau = 0$ and becomes steeper with U for a fixed U_{eff} .

Next, we clarify the effect of the two different interactions on the phase diagram. In Fig. 2 we plot T_c as a function of $-U_{\text{eff}}$. Panel (a) illustrates the effect of the

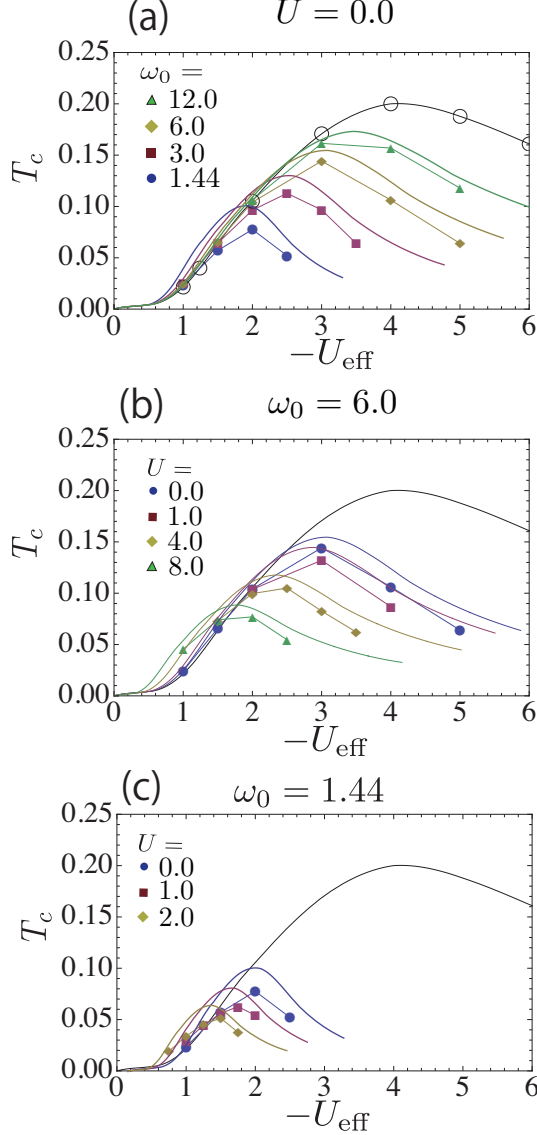


FIG. 2: T_c against $-U_{\text{eff}}$ for various sets of parameter values. (a) shows the dependence on ω_0 for $U = 0$. The lines connecting symbols are guides for the eye. The unfilled circle show the results for the attractive Hubbard model, and the black curve indicates T_c of it. (b), (c) show the phase diagram when U is switched on with a fixed value of $\omega_0 = 6$ (b), or $\omega_0 = 1.44$ (c). The colored curves show the results from the effective model.

retardation (controlled by ω_0) on the SC phase for the case $U = 0$. As ω_0 decreases, the position of the peak in T_c shifts to the weak- $|U_{\text{eff}}|$ regime, while the height of the peak decreases. We also note that the T_c in the weak-coupling regime still agrees well with that of the attractive Hubbard model with interaction U_{eff} . Let us compare this results with the behavior of CO in the Holstein model.^{32,33} The shift of the T_c dome with ω_0 is also observed in CO, while the height of the T_c peak does

not show significant change. Further, the transition temperature increases in the weak-coupling regime when U_{eff} is fixed and ω_0 decreases in CO.^{32,33} The difference between SC and CO in the weak-coupling region can be explained as follows. The important interaction for SC is the interaction between electrons with opposite spins. For CO, however, the phonon mediated interaction between electrons with the same spin is also relevant, as can be understood from a mean-field analysis in the adiabatic limit (see Appendix). When the phonon frequency is reduced, the lattice distortion takes so much time that an electron starts to feel the attraction from another electron having the same spin through this distortion. Due to this additional attraction, T_c increases in CO when ω_0 decrease, while SC does not take this advantage.

In Fig. 2(b) and (c), the effect of the Coulomb repulsion is illustrated. As U increases, the position of the peak shifts to the weak-coupling regime and the height of the peak decreases. It turns out that the T_c in the weak-coupling region is not necessarily well reproduced by the attractive Hubbard model with interaction strength U_{eff} (see e. g. $U = 8$ in panel(b) or $U = 2$ in panel (c)).

Let us now examine the above properties in terms of the low-energy effective static model in the polaron representation, which is a Hubbard model with interaction U_{eff} and a renormalized hopping parameter (reduced by the factor Z_B , see Eq. (11)). The resulting transition temperature qualitatively well describes the dependence of the transition temperature on ω_0 , U , and λ , see colored curves in Fig. 2. The effective model somewhat overestimates the transition temperature. An increase in U or a decrease in ω_0 with U_{eff} fixed leads to an increase of $Z_B = \exp(-\frac{\lambda}{2\omega_0})$, since $\lambda = U - U_{\text{eff}}$. Therefore, the band renormalization for the polaron enhances the effect of interactions between polarons, which may be characterized by the ratio between U_{eff} and the bare polaron band width $Z_B W$, where $W = 4t$ is the band width of bare electrons. As a result, the peak of the transition temperature shifts to smaller $|U_{\text{eff}}|$. Note that the effective model also shows that with larger U , the deviations from the attractive Hubbard model (black lines in Fig. 2) increase in the weak-coupling regime, see for example the colored lines for $U = 8$ in Fig. 2(b) or $U = 2$ in Fig. 2(c). This is related to the fact that the shape of T_c in the attractive Hubbard model is convex in the weak-coupling (BCS) regime. Therefore, the enhancement of the correlation due to the renormalization of the hopping parameter by Z_B can lead to deviations from the attractive Hubbard model if we do not rescale the U -axis. Here one may wonder why, when ω_0 is changed with $U = 0$ and U_{eff} fixed, the deviation from the attractive Hubbard model is not so apparent than when U is changed with ω_0 and U_{eff} fixed. This is because we need smaller ω_0 to realize a given value of Z_B when $U = 0$, while the reliability of the effective model is degraded for smaller ω_0 .

In order to estimate in which region the effective model agrees with the Holstein-Hubbard model, we plot the phase diagram in terms of the rescaled $\tilde{U}_{\text{eff}} \equiv U_{\text{eff}}/Z_B$ and rescaled $\tilde{T} \equiv Z_B T$ in Fig. 3. If the effective model reproduces the result of the Holstein-Hubbard model, the phase diagram in the space of \tilde{T} and \tilde{U}_{eff} should coincide with that of the attractive Hubbard model. Our numerical results cover the range $6 \gtrsim \tilde{U}_{\text{eff}} \gtrsim 2$. As expected,

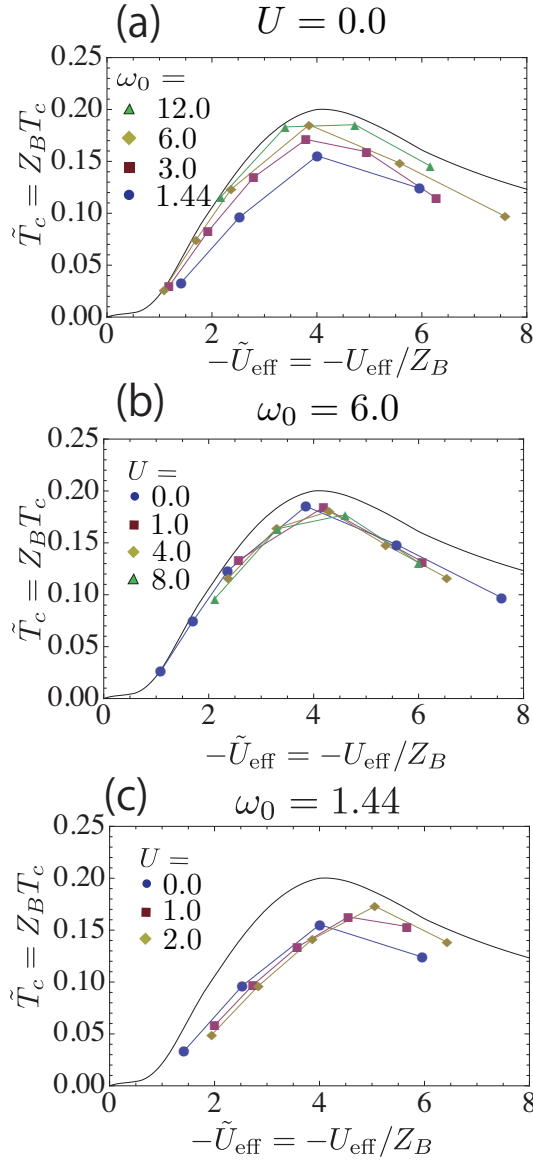


FIG. 3: The phase diagram with rescaled parameters: $\tilde{U}_{\text{eff}} \equiv U_{\text{eff}}/Z_B$ and $\tilde{T} \equiv Z_B T$. (a) shows the result for various values of ω_0 at $U = 0$. (b) (c) are the result when U is switched on with a fixed $\omega_0 = 6$ (b), or $\omega_0 = 1.44$ (c). A black curve in each panel shows T_c in the attractive Hubbard model.

the reliability of the effective model becomes better as ω_0 increases (Fig. 3 (a)). For $U = 0$, the relative deviation ($\delta T_c \equiv |T_c - T_{c,\text{eff}}|/T_c$, where $T_{c,\text{eff}}$ is defined in Eq. 13.) is smallest at intermediate coupling ($\tilde{U}_{\text{eff}} \sim 4$) for each ω_0 . The deviation decreases from $\delta T_c \leq 0.25$ for $\omega_0 = 4$ to $\delta T_c \leq 0.1$ for $\omega_0 = 12$. The dependence of δT_c on U_{eff} is relatively small at $\omega_0 \geq 4$. On the other hand, if $\omega_0 \leq 2$, the reliability of the effective model deteriorates with increasing U_{eff} , as shown in Fig. 3(a). As for the effect of U , we find that δT_c slightly, but systematically increases with increasing U , at least in the weak-coupling regime (panels (b) and (c)), and at $\omega_0 = 4$, $\delta T_c \leq 0.25$ up to $U = 4$. The effective model is quantitatively accurate

up to larger values of U for larger ω_0 .

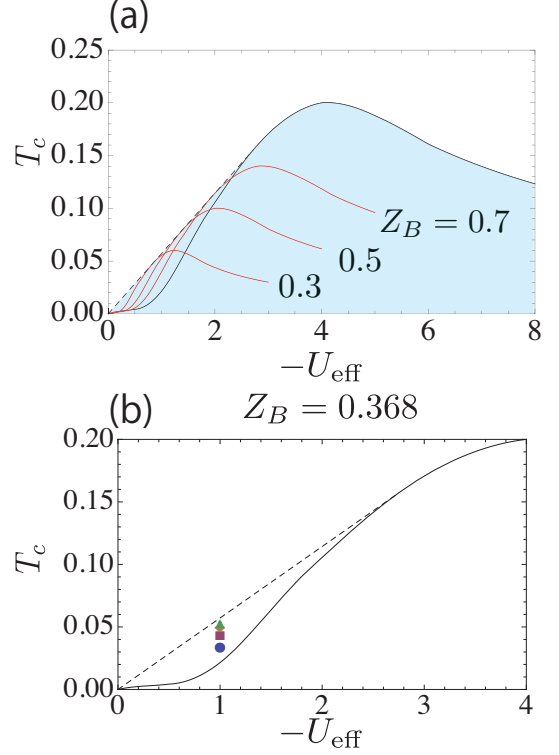


FIG. 4: (a) Possible area (shaded) for the transition temperature in the Holstein-Hubbard model, which is an envelope of the T_c curves (red) for various values of Z_B . (b) T_c vs $-U_{\text{eff}}$ for various values of ω_0 , plotted here for $U_{\text{eff}} = -1$, $Z_B = U_{\text{eff}}/U_0$.

The above analysis enables us to discuss the region in the T versus $-U_{\text{eff}}$ space where a superconducting phase of the Holstein-Hubbard model can exist. The shaded area in Fig. 4(a) shows this region as predicted by the effective model. The boundary of this area defines an envelope for the various T_c curves, which rises from the origin linearly and touches the T_c curve of the attractive model before the peak. This is because a set of T_c curves for various values of Z_B form a homologous series of phase boundaries of the attractive Hubbard model, Eq. (13). In the weak-coupling regime of the Hubbard model, the phase boundary is convex, while the boundary is concave in the intermediate regime, where the BCS-BEC crossover occurs. The envelope indeed becomes a tangent to the original curve (black solid line in Fig. 4) at $U_{\text{eff}} \simeq -2.72 \equiv U_0$. The boundary of the blue area is obtained by fixing U_{eff} , $Z_B = U_{\text{eff}}/U_0$ and taking the limit $\omega_0 \rightarrow \infty$, see Fig. 4. The effective model always overestimates the transition temperature in the parameter region studied here, so that we expect that the superconducting phase of the Holstein-Hubbard model is contained within the blue area. Here, we note that when we take the limit $\omega_0 \rightarrow \infty$ with U_{eff} , Z_B fixed, $U_{\text{eff}}(\omega) \rightarrow U_{\text{eff}}$ for every finite ω , but because $\lambda \rightarrow \infty$, this does not mean that the Holstein-Hubbard model becomes the attractive Hubbard model without bandwidth reduction.

Next we discuss the properties of the superconducting state itself. Here we focus on the temperature depen-

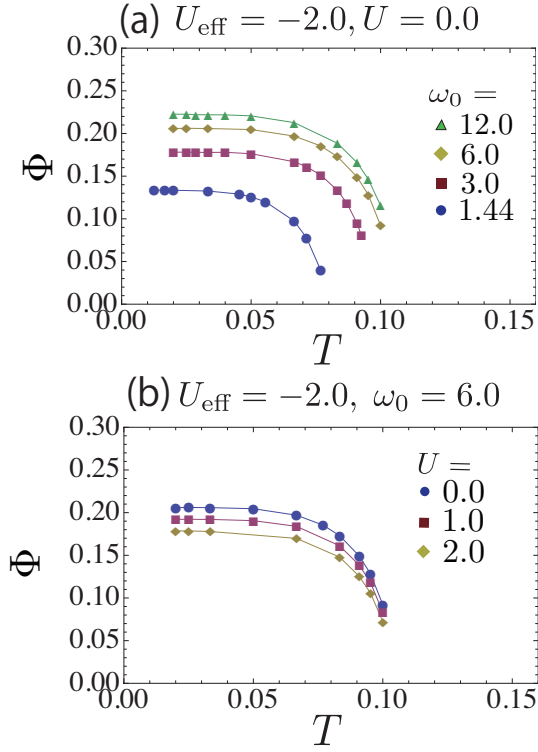


FIG. 5: Temperature dependence of the superconducting order parameter ($\Phi(T)$) for $U_{\text{eff}} = -2$, $U = 0$ with various values of ω_0 (a), or for $U_{\text{eff}} = -2$, $\omega_0 = 6$ with various values of U (b).

dence of the superconducting order parameter, $\Phi(T)$. In Fig. 5(a) we fix $U = 0$, $U_{\text{eff}} = -2$ and change the value of ω_0 . In Fig. 5(b) we fix $\omega_0 = 6$, $U_{\text{eff}} = -2$ and change U . We find that Φ monotonically increases below T_c , and saturates as temperature is decreased. As can be seen in panels (a) and (b), the retardation and the Coulomb repulsion U both act to decrease $\Phi(T)$.

In order to investigate the effect of the two types of interactions on the superconducting order parameter more systematically, we focus on the value of Φ in the limit of $T \rightarrow 0$ (Fig. 6). In panel (a), $\Phi(T \rightarrow 0)$ is plotted as a function of $-U_{\text{eff}}$. In the attractive Hubbard model, $\Phi(T \rightarrow 0)$ saturates at 0.5 in the strong coupling limit.³⁴ On the other hand, for finite ω_0 , we find that it has a peak as a function of $-U_{\text{eff}}$. Furthermore, the peak shifts to smaller $|U_{\text{eff}}|$ as the retardation increases (ω_0 decreases) or the Coulomb interaction U increases. We also note that, in the region investigated ($-U_{\text{eff}} \gtrsim 1.5$), $\Phi(T \rightarrow 0)$ decreases as ω_0 decreases or U increases, as illustrated in Fig. 5. It turns out that this behavior is qualitatively well described by the effective model, see the color lines in Fig. 6(a).

We can also explain the origin of the peak structure in $\Phi(T \rightarrow 0)$ as follows. Within the effective model, what saturates at large U_{eff} for $\omega_0 \neq 0$ is the density of pairs of polarons, which can be expressed as $\langle c_{\downarrow} c_{\uparrow} \rangle_{\text{LF}}$ after the Lang-Firsov transformation, while Φ , the order parameter defined for electrons, has some correction coming from the phonon dressing. This correction becomes large as

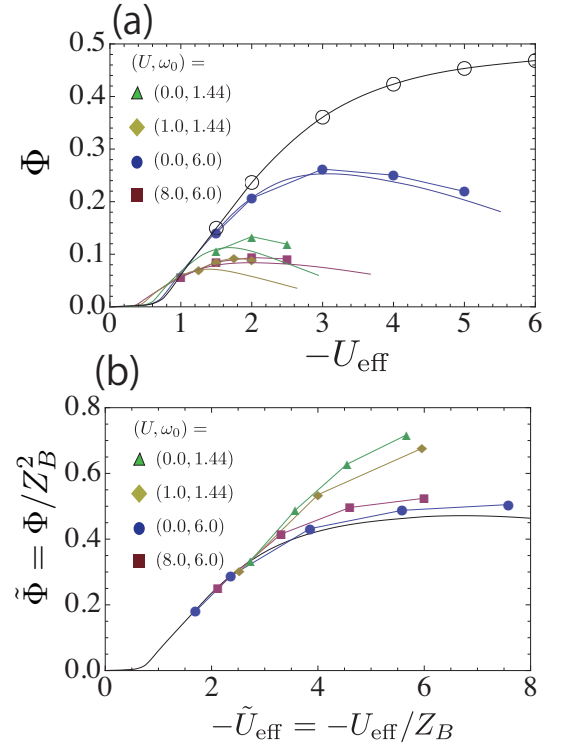


FIG. 6: The superconducting order parameter at $T = 0$ ($\Phi(T \rightarrow 0)$). Panel (a) plots the result against $-U_{\text{eff}}$ for various sets of parameter values. The unfilled circles are $\Phi(T \rightarrow 0)$ for the attractive Hubbard model, and the black curve show the interoperation of them. Panel (b) plots the result against rescaled quantities: $\tilde{U}_{\text{eff}} \equiv U_{\text{eff}}/Z_B$ and $\tilde{\Phi} \equiv \Phi/Z_B^2$.

the electron-phonon coupling becomes large, see Eq. (12) (Z_B decreases as λ increases). Related to the discussion of Fig. 5, we also have to note that the effective model, in the weak-coupling region, predicts that there is some area where $\Phi(T \rightarrow 0)$ increases as ω_0 decreases or U increases. However, within our approach (CT-QMC based on the hybridization expansion), this region is difficult to access, since it is in the weak-coupling regime and at very low temperature.

In order to assess the potential of the effective model to reproduce the superconducting order parameter, we rescale the axis of Fig. 6(a) into $\tilde{U}_{\text{eff}} \equiv U_{\text{eff}}/Z_B$ and $\tilde{\Phi} \equiv \Phi/Z_B^2$, and show the result in Fig. 6(b). Again we focus on the range $2 \lesssim -\tilde{U}_{\text{eff}} \lesssim 6$. It turns out that, with large enough $|\tilde{U}_{\text{eff}}|$, the rescaled curve underestimates $\Phi(T \rightarrow 0)$, while for smaller $|\tilde{U}_{\text{eff}}|$ ($\lesssim 2.5$), the effective model becomes better. A larger U leads to a larger underestimation in the strong $|\tilde{U}_{\text{eff}}|$ regime. Quantitatively, $\delta\Phi \equiv |(\Phi(T \rightarrow 0) - \Phi_{\text{eff}}(T \rightarrow 0))|/\Phi(T \rightarrow 0) \leq 0.2$ for $\omega_0 \gtrsim 4$ at $U = 0$, where Φ_{eff} is defined in Eq. (12). As for the effect of U , we find $\delta\Phi \leq 0.2$ up to $U = 6$ at $\omega_0 = 4$. The effective model is quantitatively accurate up to larger U for larger ω_0 . The reliability of the effective model for Φ is slightly better than in the case of the transition temperature.

Now let us move on to discuss the energy gap in the spectral function and its relation with the transition temperature. We express the self-energy, which is independent of momentum in DMFT, as

$$\hat{\Sigma}(i\omega_n) = \begin{bmatrix} \Sigma(i\omega_n) & S(i\omega_n) \\ S(i\omega_n) & -\Sigma^*(i\omega_n) \end{bmatrix}, \quad (18)$$

where Σ is the normal self-energy while S is the anomalous one. Then the lattice Green's function in momentum space is

$$\begin{aligned} \hat{G}(\mathbf{k}, i\omega_n) &= \begin{bmatrix} G_{11}(\mathbf{k}, i\omega_n) & G_{12}(\mathbf{k}, i\omega_n) \\ G_{21}(\mathbf{k}, i\omega_n) & G_{22}(\mathbf{k}, i\omega_n) \end{bmatrix} \\ &= [G^0(\mathbf{k}, i\omega_n)^{-1} - \Sigma(i\omega_n)]^{-1} + [S(i\omega_n)]^2]^{-1} \times \\ &\quad \begin{bmatrix} G^0(-\mathbf{k}, -i\omega_n)^{-1} - \Sigma(-i\omega_n) & -S(i\omega_n) \\ -S(i\omega_n) & -G^0(\mathbf{k}, i\omega_n)^{-1} + \Sigma(i\omega_n) \end{bmatrix}, \end{aligned} \quad (19)$$

where $G^0(\mathbf{k}, i\omega_n) = i\omega_n - (\epsilon_{\mathbf{k}} - \mu)$ is the bare lattice Green's function and $\epsilon_{\mathbf{k}}$ the dispersion relation for the bare electrons. With Dyson's equation and Eq. (9), one finds for the Bethe lattice that

$$\hat{\Sigma}(i\omega_n) = i\omega_n \sigma_0 + \mu \sigma_3 - t^2 \sigma_3 \hat{G}_{\text{loc}}(i\omega_n) \sigma_3 - \hat{G}_{\text{loc}}^{-1}(i\omega_n), \quad (20)$$

where σ_0 is the identity matrix. As long as the Fermi liquid picture is valid, we can express the self-energies for small $|\omega_n|$ as

$$\Sigma(i\omega_n) = \Sigma^{(0)} + i\omega_n \Sigma^{(1)} + O((i\omega_n)^2), \quad (21)$$

$$S(i\omega_n) = S^{(0)} + O((i\omega_n)^2), \quad (22)$$

where $\Sigma^{(0)}$, $\Sigma^{(1)}$, $S^{(0)}$ are real, and $Z = (1 - \Sigma^{(1)})$ denotes the Matsubara-axis mass-renormalization factor. Neglecting the $O((i\omega_n)^2)$ term in Eq. (22), inserting the expansions into Eq. (19) and making an analytic continuation, one finds that the gap in the excitation spectrum is

$$\Delta \equiv S^{(0)}/Z. \quad (23)$$

This provides a rough estimate of the spectral gap. In the BCS theory, the ratio between the energy gap and the transition temperature ($2\Delta(T \rightarrow 0)/T_c$) is 3.528, so that any deviation from this value is a measure for the deviation from the BCS theory.

We plot these quantities in Fig. 7. Here we use the approximations $\Sigma^{(1)} \approx \text{Im}\Sigma(\omega_{n=0})/\omega_{n=0}$, and $S^{(0)} \approx (9S(\omega_{n=0}) - S(\omega_{n=1}))/8$. The gap parameter for $T \rightarrow 0$, $\Delta(T \rightarrow 0)$, is shown in Fig. 7(a). It turns out that it monotonically increases with $|U_{\text{eff}}|$. When we decrease ω_0 for fixed $U = 0$, $\Delta(T \rightarrow 0)$ does not necessarily change monotonically with ω_0 for each value of U_{eff} , but the dependence on ω_0 is small. When we increase U with fixed ω_0 , it increases for each $-U_{\text{eff}}$.

Fig. 7(b) plots $2\Delta(T \rightarrow 0)/T_c$. Again it monotonically increases with $|U_{\text{eff}}|$. We find that, while $2\Delta(T \rightarrow 0)/T_c$ approaches the BCS value 3.528 for $-U_{\text{eff}} \rightarrow 0$ in all the cases, there is a steep rise at a value of $|U_{\text{eff}}|$ that depends on ω_0 and U . The deviation increases when ω_0 is decreased or U is increased.

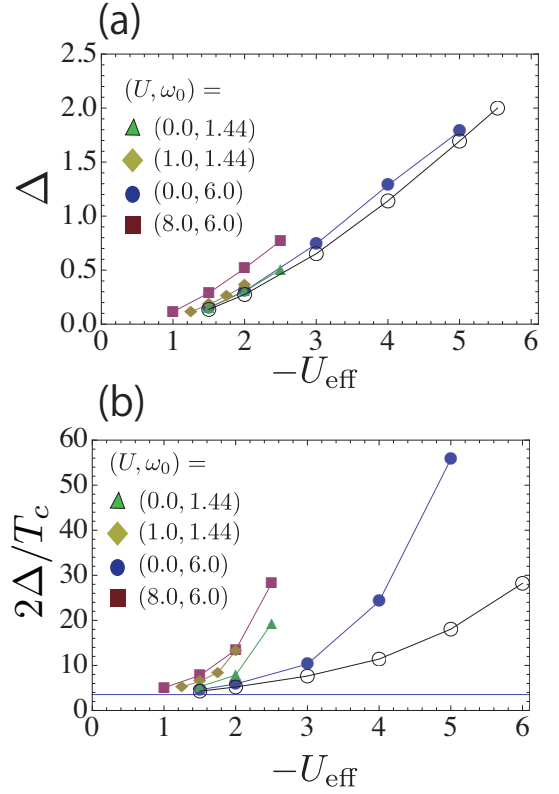


FIG. 7: (a) The energy-gap parameter $\Delta (= \Delta(T \rightarrow 0))$ against $-U_{\text{eff}}$ for various sets of parameters. (b) The ratio of the energy-gap parameter to the transition temperature ($2\Delta(T \rightarrow 0)/T_c$) against $-U_{\text{eff}}$. The horizontal blue line indicates the BCS value $2\Delta/T_c = 3.528$. The unfilled circles are the results for the attractive Hubbard model for each panel.

Finally let us discuss the possible relevance of these results for organic superconductors, such as alkali-doped fullerides and aromatic superconductors.⁴⁻⁶ In these molecular solids, the characteristic frequency of intra-molecular phonons is reported to be not larger than but comparable to the electronic bandwidth or the inverse of the density of states at the Fermi level. What we have found here is that the effective static model is qualitatively reliable even for $\omega_0 \simeq t = W/4$. Therefore, we expect that the static effective model in the polaron picture is useful to analyze the qualitative behavior, such as the dependence on pressure. We caution however that in a realistic study of organic superconductors, one has to consider multiple orbitals and different types of electron-electron and electron-phonon couplings (Hund's couplings, intra-orbital phonon couplings and/or Jahn-Teller interactions).

B. Antiferromagnetism and charge order

To understand the competition of ordered phases in the presence of two kinds of interactions, we now investigate the Holstein-Hubbard model at non-zero temperatures around $U_{\text{eff}} = 0$, without any constraint (i.e., allowing

SC, commensurate CO and commensurate AF). In the following, the order parameter of the CO phase (Φ_{CO}) is defined as $\Phi_{\text{CO}} = [(n_{A,\uparrow} + n_{A,\downarrow}) - (n_{B,\uparrow} + n_{B,\downarrow})]/4$, where $n_{A,\sigma}$ ($n_{B,\sigma}$) represents the density of electrons on the A (B) sublattice with spin σ . For the AF phase the order parameter is defined as $\Phi_{\text{AF}} = (n_{\uparrow} - n_{\downarrow})/2$, where n_{\uparrow} (n_{\downarrow}) is the density of up-spin (down-spin) electrons. To obtain the data points, we use the hybridization functions for $U_{\text{eff}} = U - \lambda$ as an input for the next step $U_{\text{eff}} = U - \lambda - \delta\lambda$, where $\delta\lambda$ denotes a small increment in λ .

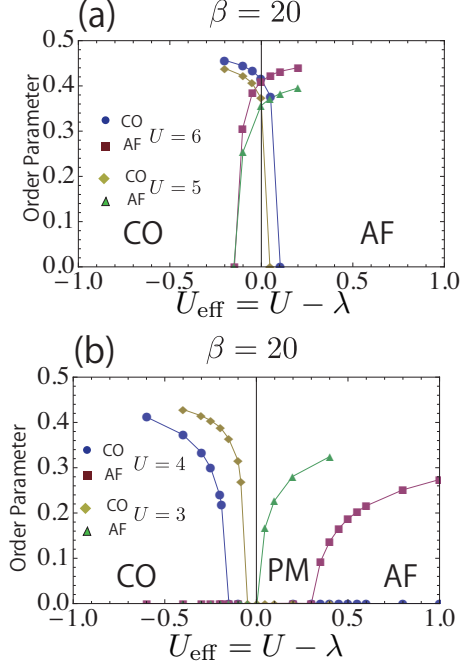


FIG. 8: Order parameters against $U_{\text{eff}} = U - \lambda$ around $U \sim \lambda$ for a fixed $\omega_0 = 0.6$ at half-filling. In panel (a), the result for $U = 6, 5$ is shown, while in panel (b) the result for $U = 4, 3$, both at $\beta = 20$. For smaller U , the charge ordered state (CO) and the antiferromagnetic phase (AF) are separated by a paramagnetic metallic phase (PM).

Figure 8 shows the behavior of the order parameters around $U_{\text{eff}} = 0$, which has been obtained by varying λ to change U_{eff} for each value of U . Here we fix $\omega_0 = 0.6$ and $\beta = 20$. There is no SC phase, and AF and CO compete with each other. If the interaction U is strong enough ($U = 5, 6$, see Fig. 8(a)), the phase transition is of first order i.e., the order parameters show a hysteresis around the phase boundary. In other words, there is a region around $U_{\text{eff}} = 0$, in which both an AF and a CO solution of the DMFT equations exists. In order to determine the stable solution, one would have to compare the free energies. On the other hand, if the interaction U is smaller ($U = 3, 4$, see Fig. 8(b)), a paramagnetic metallic phase (PM) appears between the CO and AF phase. The transition to PM is second order, since the order parameter continuously goes to 0 as one approaches the boundary Fig. 8.

We can summarize the results by plotting the phase diagrams in the U - λ plane for various conditions in Fig. 9 and by plotting the phase diagrams in the U - $-U_{\text{eff}}$ in

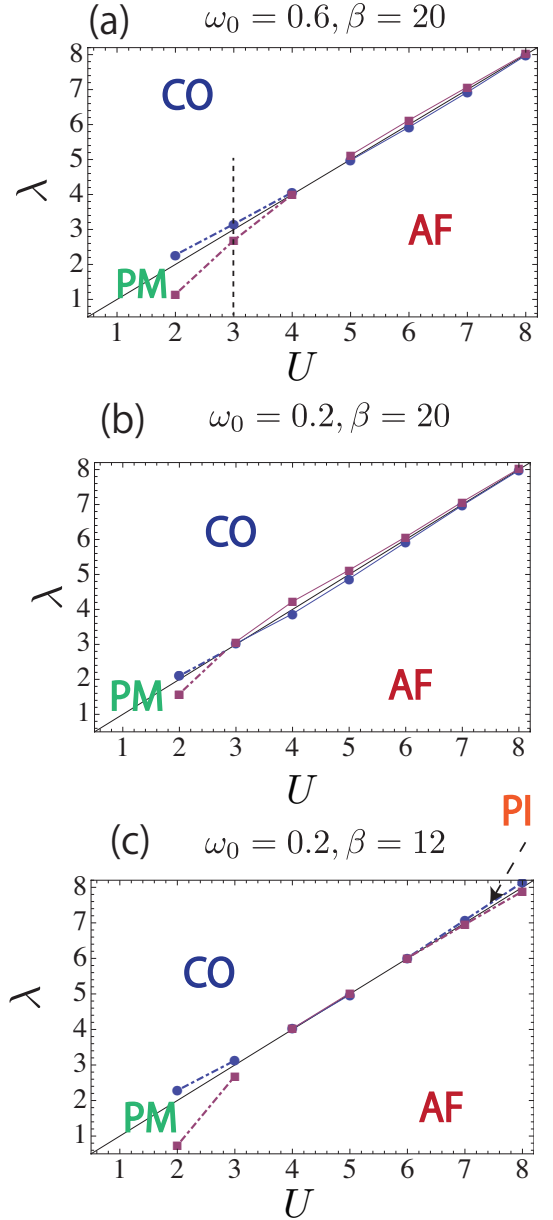


FIG. 9: Finite temperature phase diagram in the U - λ plane. On top of charge ordered state (CO), antiferromagnetic phase (AF), CO, AF and paramagnetic metallic phase (PM), PI stands for a paramagnetic insulating state. Colored dotted lines represent the boundary between a paramagnetic phase and ordered phases, which is continuous. Solid lines show the boundary of the region where the stable solution for CO or AF exists. For each type of lines, the red line shows the boundary of AF and blue line is for CO.

Fig. 10(a)(b). In the weak coupling regime, as pointed out above, there is a paramagnetic metallic phase (PM) around $U_{\text{eff}} = 0$. It turns out that the area of the PM phase is wider on the $U > \lambda$ side than on the opposite side. This can be explained by a mean-field theory in the adiabatic limit, which has been used to explain the first-order transition in the strong coupling regime at

$T = 0$ in Ref. 20. This approximation shows that the interaction that appears in the gap equation is $U - 2\lambda$ for CO and U for AF, as elaborated in the Appendix, and this explains the different extents of the two regions. The paramagnetic metallic phase between AF and CO is also expected in the anti-adiabatic limit, where the HH model becomes the Hubbard model with interaction U_{eff} . Ref. 20 pointed out that the nature of this limit shows up in the weak-coupling regime as a continuous transition between AF and CO. In that sense, the present result is consistent with Ref. 20. However, we note that the Hubbard model cannot explain the difference in the extent of the PM region between $U > \lambda$ and $U < \lambda$, since the Hubbard model solution should be symmetric around the line $U = \lambda$. In the intermediate-coupling regime, the transition between AF and CO is of first-order and takes place within the hysteretic region, see Fig. 10(a)(b) for more details. This hysteretic region of two solutions (AF and CO) is located near $U \sim \lambda$ even at non-zero temperatures, and is shown as the region surrounded by red and blue solid lines in Fig. 9 and in Fig. 10(a)(b). This result agrees with the results at $T = 0$.^{19,20} We also find that, in the strong-coupling regime, the hysteretic region becomes narrower with larger U (or λ) (Fig. 9 (a)(b), Fig. 10(a)). In the large- U regime, the CO and AF solutions are separated by a paramagnetic insulating phase (Fig. 9(c), Fig. 10(b)). When we compare the different panels, we find that the region of paramagnetic states is suppressed as the temperature decreases (compare Figs. 9(b) and (c)) or as ω_0 decreases (compare Figs. 9(a) and (b)). The latter may be because the cancellation of the instantaneous repulsive interaction and the retarded interaction is more direct than in the case of smaller ω_0 .

Finally, we show the evidence for the metallic nature of the PM phase in the small- U regime. We use the relation between the Green's function on the imaginary axis and the spectral function ($A(\omega) = -\frac{1}{\pi}\text{Im}G_{\text{loc}}(\omega)$),

$$G(\tau = \beta/2) = - \int d\omega \frac{1}{2 \cosh(\beta\omega/2)} A(\omega). \quad (24)$$

If the temperature is low enough, $1/\cosh(\beta\omega/2)$ has a strong peak at $\omega = 0$. Then the value of $-\frac{\beta}{\pi}G(\tau = \beta/2)$ gives a good estimate of the value of $A(\omega = 0)$. The result is shown in Fig. 10(c) for $U = 3$, $\mu = 1.5$, and indicates that there is indeed a significant density of states at the Fermi level in the PM phase. Note that we can only observe a small value of $-\frac{\beta}{\pi}G(\tau = \beta/2)$ in the paramagnetic state in the strong coupling regime, so that this phase must be regarded as a paramagnetic insulating phase.

IV. CONCLUSION

We have systematically investigated the effect of the electron-electron interaction and the electron-phonon coupling on the ordered states of the half-filled Holstein-Hubbard model, using DMFT and CT-QMC. In the study of the superconducting state, we have found that the interplay of the Coulomb interaction and the retarded attractive interaction leads to a nontrivial structure in

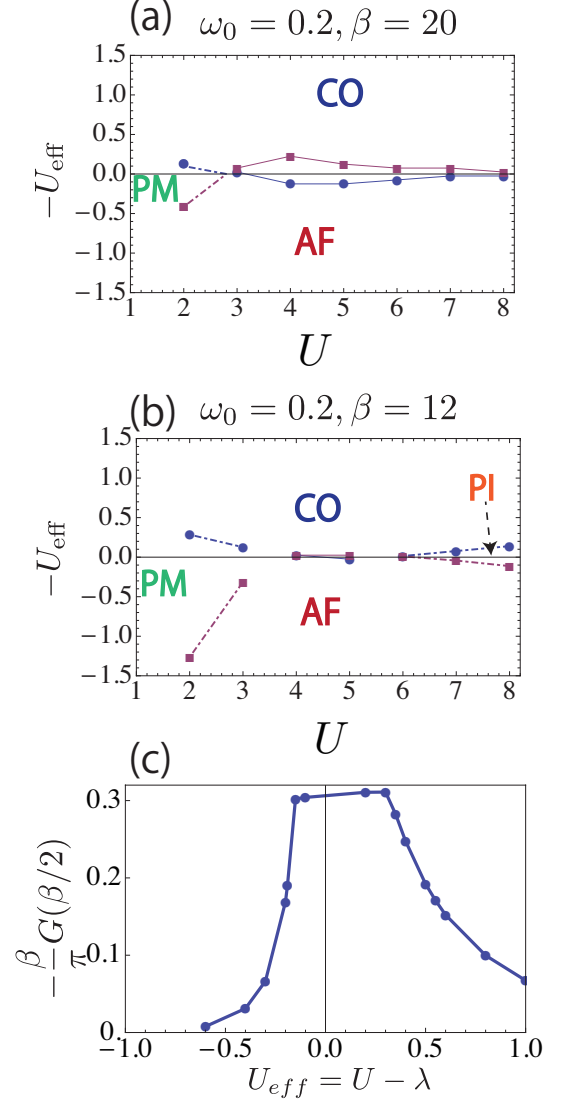


FIG. 10: (a)(b) Finite temperature phase diagram in the U - U_{eff} plane. Colored dotted lines represent the boundary between a paramagnetic phase and ordered phases, which is continuous. Solid lines show the boundary of the region where the stable solution for CO or AF exists. For each type of lines, the red line shows the boundary of AF and blue line is for CO. (c) $-\frac{\beta}{\pi}G(\tau = \beta/2)$ against U_{eff} with a fixed $U = 3$ (vertical dotted line in Fig. 9(a)) with $\mu = 1.5, \omega_0 = 0.6$.

the anomalous Green's functions, and we have shown that the maximum transition temperature decreases as a result of the electron-phonon interaction and shifts to the small U_{eff} regime. The superconducting order parameter shows a similar behavior. We have explained these observations with an effective static model derived from a Lang-Firsov decoupling and a projection onto the zero-boson subspace, and we have investigated the accuracy and reliability of the effective model. We have also discussed the region where a SC state can be realized in the HH model in the T_c -versus- U_{eff} phase diagram. Finally, we have investigated the HH model at $T > 0$

around $U_{\text{eff}} = 0$, allowing for SC, AF and CO phases. A paramagnetic phase (PM) appears between CO and AF in the weak-coupling region and a paramagnetic insulating phase (PI) for strong enough coupling, while in the intermediate-coupling regime, the transition between CO and AF is direct and discontinuous and a hysteresis region of AF and CO is located around $U_{\text{eff}} = 0$ at non-zero temperatures.

Acknowledgments

The authors would like to thank T. Kariyado, T. Oka, M. Tezuka and A. Koga for constructive advice and discussion. The simulations in this study have been performed using some of the ALPS libraries (Ref. 35).

Appendix A: Static mean-field treatment for AF and CO

We briefly discuss a static mean-field theory for a heuristic understanding of the behavior of CO and AF. We treat both interactions in Eq. (1) with a mean-field approximation by introducing the average of the lattice displacement $\langle b_i^\dagger + b_i \rangle / \sqrt{2\omega_0}$ and the averaged density $\langle n_{i,\sigma} \rangle$. The mean-field Hamiltonian is decomposed as

$$H_{\text{MF}} \equiv H_{\text{MF}}^e + H_{\text{MF}}^{ph}, \quad (\text{A1})$$

where

$$H_{\text{MF}}^e = -t \sum_{\langle i,j \rangle, \sigma} [c_{j,\sigma}^\dagger c_{i,\sigma} + H.c.] + \sum_i [U(\langle n_{i\uparrow} \rangle n_{i\downarrow} + \langle n_{i\downarrow} \rangle n_{i\uparrow}) - \mu n_i + g(\langle b_i^\dagger + b_i \rangle n_i)], \quad (\text{A2})$$

and

$$H_{\text{MF}}^{ph} = g \sum_i (\langle b_i^\dagger + b_i \rangle (\langle n_i \rangle - 1) + \omega_0 \sum_i b_i^\dagger b_i). \quad (\text{A3})$$

From H_{MF}^{ph} , we find $\langle b_i \rangle = \langle b_i^\dagger \rangle = -\frac{g}{\omega_0} (\langle n_i \rangle - 1)$. Then we obtain

$$H_{\text{MF}}^e = -t \sum_{\langle i,j \rangle, \sigma} [c_{j,\sigma}^\dagger c_{i,\sigma} + H.c.] - \sum_i (\mu - \lambda) n_i + \sum_{i,\sigma} n_{i\sigma} (U \langle n_{i\bar{\sigma}} \rangle - \lambda \langle n_i \rangle). \quad (\text{A4})$$

This Hamiltonian shows that the effective attractive interaction, $-n_{i\sigma} \lambda \langle n_i \rangle$, comes from electrons of both spins, which is different from the case of the Coulomb interaction. In the following, let us focus on half-filling and consider the solution of CO and AF.

For CO, $\langle n_{A\uparrow} \rangle = \langle n_{A\downarrow} \rangle \neq \langle n_{B\uparrow} \rangle = \langle n_{B\downarrow} \rangle$. We define the order parameter as $\Phi_{\text{CO}} = (\langle n_{A\uparrow} \rangle - \langle n_{B\uparrow} \rangle)/2$. On the other hand, for AF, $\langle n_{A\uparrow} \rangle = \langle n_{B\downarrow} \rangle \neq \langle n_{A\downarrow} \rangle = \langle n_{B\uparrow} \rangle$. We define the order parameter as $\Phi_{\text{AF}} = (\langle n_{A\uparrow} \rangle - \langle n_{A\downarrow} \rangle)/2$. Then we obtain a self-consistent equation,

$$1 = V \int d\xi \rho(\xi) \frac{\tanh(\beta E(\xi, \Phi, V)/2)}{2E(\xi, \Phi, V)}, \quad (\text{A5})$$

where $\rho(\xi)$ is the density of states for bare electrons and $E(\xi, \Phi, V) = \sqrt{V^2 \Phi^2 + \xi^2}$. For CO we put $\Phi = \Phi_{\text{CO}}$, $V = |U - 2\lambda|$ and for AF, $\Phi = \Phi_{\text{AF}}$, $V = |U|$.

Note that if we consider CO and SC in the attractive Hubbard model within the static mean-field approximation, we put $V = |U| = |U_{\text{eff}}|$ in Eq. (A5). On the other hand, when we consider the Holstein model, we use $V = 2|\lambda| = 2|U_{\text{eff}}|$, which corresponds to the effective interaction for both spin up and down. This explains why the transition temperature for CO is enhanced in the small U_{eff} regime as ω_0 decreases, which was pointed out in Refs. 32,33.

We also note that the static mean-field analysis can explain the reason why the PM region is larger on the $U > \lambda$ side than on the $U < \lambda$ side. This comes from the different dependence of AF and CO on U and λ . At a given temperature T , let $V_0 > 0$ satisfy

$$1 = V_0 \int d\xi \rho(\xi) \frac{\tanh(\beta E(\xi, 0, V_0)/2)}{2E(\xi, 0, V_0)}. \quad (\text{A6})$$

The mean-field analysis then dictates that the boundary of CO and PM is located at $\lambda = (V_0 + U)/2$, while the boundary of AF and PM is at $U = V_0$. The two boundaries cross at $U = \lambda = V_0$, and a first-order transition occurs for $U, \lambda > V_0$.

¹ A. Lanzara, P. V. Bogdanov, X. J. Zhou, S. A. Kellar, D. L. Feng, E. D. Lu, T. Yoshida, H. Eisaki, A. Fujimori, K. Kishio, J. I. Shimoyama, T. Noda, S. Uchida, Z. Hussain and Z. X. Shen, *Nature* **412**, 510 (2001).

² Y. Takabayashi, A. Y. Ganin, P. Jeglic, D. Arcon, T. Takano, Y. Iwasa, Y. Ohishi, M. Takata, N. Takeshita, K. Prassides, and M. J. Rosseinsky, *Science* **323**, 1585 (2009).

³ M. Capone, M. Fabrizio, C. Castellani, and E. Tosatti, *Rev. Mod. Phys.* **81**, 943 (2009).

⁴ O. Gunnarsson, *Rev. Mod. Phys.* **69**, 575 (1997).

⁵ T. Kato, T. Kambe, and Y. Kubozono, *Phys. Rev. Lett.* **107**, 077001 (2011).

⁶ A. Subedi and L. Boeri, *Phys. Rev. B* **84**, 020508(R) (2011).

⁷ Y. Nomura, K. Nakamura, and R. Arita, *Phys. Rev. B* **85**, 155452 (2012).

⁸ M. Tezuka, R. Arita, and H. Aoki, *Phys. Rev. Lett.* **95**, 226401 (2005) ; *Phys. Rev. B* **76**, 155114 (2007).

- ⁹ H. Fehske, G. Hager and E. Jeckelmann, Europhys. Lett. **84**, 57001(2008).
- ¹⁰ R. T. Clay and R. P. Hardikar, Phys. Rev. Lett. **95**, 096401(2005).
- ¹¹ W. Metzner and D. Vollhardt, Phys. Rev. Lett. **62**, 324 (1989).
- ¹² A. Georges and G. Kotliar, Phys. Rev. B **45**, 6479 (1992).
- ¹³ A. Georges, G. Kotliar, W. Krauth, and M. J. Rozenberg, Rev. Mod. Phys. **68**, 13 (1996).
- ¹⁴ P. Werner and A. J. Millis, Phys. Rev. Lett. **99**, 146404 (2007).
- ¹⁵ W. Koller, D. Meyer, Y. Ono and A. C. Hewson, Europhys. Lett. **66**, 559 (2004).
- ¹⁶ G. Sangiovanni, M. Capone, C. Castellani, and M. Grilli, Phys. Rev. Lett. **94**, 026401 (2005).
- ¹⁷ W. Koller, A. C. Hewson, and D. M. Edwards, Phys. Rev. Lett. **95**, 256401(2005).
- ¹⁸ J. K. Freericks and M. Jarrell, Phys. Rev. Lett. **75**, 2570 (1995).
- ¹⁹ J. Bauer, EPL **90**, 27002 (2010).
- ²⁰ J. Bauer and A. C. Hewson, Phys. Rev. B **81**, 235113 (2010).
- ²¹ J. Bauer, J. E. Han, and O. Gunnarsson, Phys. Rev. B **84**, 184531 (2011).
- ²² J. Bauer, J. E. Han, and O. Gunnarsson, Phys. Rev. B **87**, 054507 (2013).
- ²³ A. B. Migdal, Sov. Phys. JETP **7**, 996 (1958).
- ²⁴ G. M. Eliashberg, Sov. Phys. JETP **11**, 696 (1960) ; **12**, 1000 (1961).
- ²⁵ W. L. McMillan, Phys. Rev. **125** 331 (1968).
- ²⁶ M. Casula, P. Werner, L. Vaugier, F. Aryasetiawan, T. Miyake, A. J. Millis, and S. Biermann, Phys. Rev. Lett. **109**, 126408 (2012).
- ²⁷ J. T. Devreese and A. S. Alexandrov, Rep. Prog. Phys. **72**, 066501 (2009).
- ²⁸ A. S. Alexandrov and N. F. Mott, Rep. Prog. Phys. **57**, 1197 (1994).
- ²⁹ P. Werner, A. Comanac, L. de'Medici, M. Troyer, and A. J. Millis, Phys. Rev. Lett. **97**, 076405 (2006).
- ³⁰ E. Gull, A. J. Millis, A. I. Lichtenstein, A. N. Rubtsov, M. Troyer, and P. Werner, Rev. Mod. Phys. **83**, 349 (2011).
- ³¹ I. G. Lang and Y. A. Firsov, Sov. Phys. JETP **16**, 1301 (1962).
- ³² J. K. Freericks et al, Europhys. Lett. **25**, 37 (1994).
- ³³ J. K. Freericks, M. Jarrell, and D. J. Scalapino, Phys. Rev. B **48**, 6302 (1993).
- ³⁴ A. Koga and P. Werner, Phys. Rev. A **84**, 023638 (2011).
- ³⁵ A. Albuquerque, F. Alet, P. Corboz, P. Dayal, A. Feiguin, S. Fuchs, L. Gamper, E. Gull, S. Gürtler, A. Honecker, R. Igarashi, M. Körner, A. Kozhevnikov, A. Läuchli, S. Manmana, M. Matsumoto, I. McCulloch, F. Michel, R. Noack, G. Pawłowski, L. Pollet, T. Pruschke, U. Schollwöck, S. Todo, S. Trebst, M. Troyer, P. Werner, and S. Wessel, J. Magn. Magn. Mater. **310**, 1187 (2007) ; B. Bauer, L. D. Carr, H. G. Evertz, A. Feiguin, J. Freire, S. Fuchs, L. Gamper, J. Gukelberger, E. Gull, S. Gürtler, A. Hehn, R. Igarashi, S. V. Isakov, D. Koop, P. N. Ma, P. Mates, H. Matsuo, O. Parcollet, G. Pawłowski, J. D. Picon, L. Pollet, E. Santos, V. W. Scarola, U. Schollwöck, C. Silva, B. Surer, S. Todo, S. Trebst, M. Troyer, M. L. Wall, P. Werner, and S. Wessel, J. Stat. Mech.: Theor. Exper. **(2011)** P05001.
- ³⁶ For the attractive Hubbard model, the treatment of the superconducting phase within DMFT and the hybridization expansion CT-QMC approach has been discussed in Ref. 34.